J|A|C|S
ARTICLES
Published on Web 03/23/2002

The Energy Landscape of Unsolvated Peptides: Helix Formation and Cold Denaturation in Ac-$A_4G_7A_4 + H^+$

Brian S. Kinnear, Matthew R. Hartings, and Martin F. Jarrold*

Contribution from the Department of Chemistry, Northwestern University, 2145 Sheridan Road, Evanston, Illinois 60208

Received September 10, 2001

Abstract: Ion mobility measurements and molecular dynamics simulations were performed for unsolvated $A_4G_7A_4 + H^+$ and Ac-$A_4G_7A_4 + H^+$ (Ac = acetyl, A = alanine, G = glycine) peptides. As expected, $A_4G_7A_4 + H^+$ adopts a globular conformation (a compact, random-looking, three-dimensional structure) over the entire temperature range examined (100−410 K). Ac-$A_4G_7A_4 + H^+$ on the other hand is designed to have a flat energy landscape with a marginally stable helical state. This peptide shows at least four different conformations at low temperatures (<230 K). The two conformations with the largest cross sections are attributed to α- and partial π-helices, while the one with the smallest cross section is globular. The other main conformation may be partially helical. Ac-$A_4G_7A_4 + H^+$ becomes predominantly globular at intermediate temperatures and then becomes more helical as the temperature is raised further. This unexpected behavior may be due to the helix having a higher vibrational entropy than the globular state, as predicted by some recent calculations (Ma, B.; Tsai, C.-J.; Nussinov, R. *Biophys. J.* **2000**, *79*, 2739−2753).

Introduction

The conformations adopted by a protein, or indeed any macromolecule, depend on its potential energy surface. The topology of the potential energy surface determines whether a polypeptide folds into a unique conformation or becomes trapped in a series of local minimums. In solution, intramolecular interactions and interactions with the solvent are both important in defining the energy landscape. It is the complex interplay between them that makes protein structure and folding such difficult problems to understand. One approach to untangling these interactions is to examine the conformations and properties of unsolvated and partially solvated peptides and proteins in the vapor phase.[1−8] Understanding the energy landscape for unsolvated peptides provides a natural starting point for understanding their behavior in the different environments that are important in real biological systems. This includes environments (such as the inside of membranes) that are very different from aqueous solution where many studies have been performed in the past. In this work, we focus on helix formation. The helix is the dominant secondary structure element in proteins, and so it is important to have a thorough understanding of the factors responsible for its stability throughout the biological milieu.

Alanine has a high helix propensity in solution,[9−12] and alanine-based peptides are usually helical in the gas phase.[13,14] Glycine has a low helix propensity in both environments,[12,15] and it is often considered to be a helix breaker. Glycine-based peptides adopt globular conformations (compact, random-looking, three-dimensional structures) in the gas phase.[15] Peptides with marginally stable helical states in vacuo can be produced by mixing glycine and alanine residues.[16] These peptides have a flattened energy landscape where the helix and globular conformations have similar energies. Here we describe studies of the conformations of unsolvated Ac-$A_4G_7A_4 + H^+$ and $A_4G_7A_4 + H^+$ (Ac = acetyl, A = alanine, G = glycine) peptides over a wide temperature range (100−410 K). On the basis of our previous studies,[13,14,16,17] Ac-$A_4G_7A_4 + H^+$ is expected to have a marginally stable helical state while $A_4G_7A_4 + H^+$ is expected to have a globular conformation. The different conformations are believed to result because of different protonation sites in the two peptides. Protonation at or near the N-terminus destabilizes the helix through unfavorable interac-

* To whom correspondence should be addressed. E-mail: mfj@chem.nwu.edu.

(1) Suckau, D.; Shi, Y.; Beu, S. C.; Senko, M. W.; Quinn, J. P.; Wampler, F. M.; McLafferty, F. W. *Proc. Natl. Acad. Sci. U.S.A.* **1993**, *90*, 790−793.
(2) Campbell, S.; Rodgers, M. T.; Marzluff, E. M.; Beauchamp, J. L. *J. Am. Chem. Soc.* **1995** *117*, 12840−12854.
(3) Schnier, P. D.; Price, W. D.; Jockusch, R. A.; Williams, E. R. *J. Am. Chem. Soc.* **1996**, *118*, 7178−7189.
(4) Kaltashov I. A.; Fenselau, C. *Proteins: Struct., Funct., Genet.* **1997**, *27*, 165−170.
(5) Valentine, S. J.; Clemmer, D. E. *J. Am. Chem. Soc.* **1997**, *119*, 3558−3566.
(6) Wyttenbach, T., Bushnell, J. E.; Bowers, M. T. *J. Am. Chem. Soc.* **1998**, *120*, 5098−5103.
(7) Arteca, G. A.; Velázquez, I.; Reimann, C. T.; Tapia, O. *Phys. Rev. E* **1999**, *59*, 5981−5986.
(8) Schaaff, T. G.; Stephenson, J. L.; McLuckey, S. L. *J. Am. Chem. Soc.* **1999**, *121*, 8907−8919.
(9) Lyu, P. C.; Liff, M. I.; Marky, L. A.; Kallenbach, N. R. *Science* **1990**, *250*, 669−673.
(10) O'Neil, K. T.; DeGrado, W. F. *Science* **1990**, *250*, 646−651.
(11) Padmanabhan, S.; Marqusee, S.; Ridgeway, T.; Laue, T. M.; Baldwin. *Nature* **1990**, *344*, 268−270.
(12) Chakrabartty, A.; Baldwin, R. L. *Adv. Protein Chem.* **1995**, *46*, 141−176.
(13) Hudgins, R. R.; Ratner, M. A.; Jarrold, M. F. *J. Am. Chem. Soc.* **1998**, *120*, 12974−12975.
(14) Hudgins, R. R.; Jarrold, M. F. *J. Am. Chem. Soc.* **1999**, *121*, 3494−3501.
(15) Hudgins, R. R.; Jarrold, M. F. *J. Phys. Chem. B* **2000**, *104*, 2154−2158.
(16) Kaleta, D. T.; Jarrold, M. F. *J. Phys. Chem. B* **2001**, *105*, 4436−4440.
(17) Kinnear, B. S.; Kaleta, D. T.; Kohtani, M.; Hudgins, R. R.; Jarrold, M. F. *J. Am. Chem. Soc.* **2000**, *122*, 9243−9256.

10.1021/ja012150v CCC: $22.00

tions between the charge and the helix macrodipole while protonation near the C-terminus stabilizes the helix by favorable charge−dipole interactions.[18−21]

The unsolvated Ac-$A_4G_7A_4 + H^+$ peptide displays a remarkably complex behavior. At low temperatures, it is found to be trapped in several different conformations ranging from an α-helix to a globule. At intermediate temperatures, Ac-$A_4G_7A_4 + H^+$ becomes globular and then it becomes more helical as the temperature is raised further. Normally, ordered states give way to disordered ones as the temperature is raised; thus, helical peptides are expected to denature as the temperature is increased. The preference for the helical state at high temperature and the denatured state at low temperature is reminiscent of the cold denaturation of proteins in solution. This phenomenon has been known for many years and is attributed to the solvation of hydrophobic groups becoming less entropically unfavorable at lower temperatures.[22] With the unsolvated peptides studied here, it appears that cold denaturation is driven by the difference in the vibrational entropy of the helical and denatured states. Some recent calculations suggest that helices have higher vibrational entropies than globules because they have low-frequency longitudinal modes for which there are no counterparts in the compact globule.[23]

In the studies described here, the unsolvated peptide ions are generated by electrospray and information about their conformations is obtained from gas-phase ion mobility measurements. The ion mobilities depend on the collision cross section, which in turn depends on the geometry.[24−26] Structural information is obtained by comparing the cross sections derived from the mobilities to cross sections calculated for trial geometries obtained from MD simulations. This approach can easily distinguish helices and globules.[27]

Experimental Methods and Materials

The experiments were performed on a new temperature-variable injected ion mobility apparatus which has been described in detail elsewhere.[28] Briefly, the apparatus consists of an electrospray source with a heated capillary interface, a 30.5-cm-long, temperature-variable drift tube, a quadrupole mass spectrometer, and a detector. The drift tube contains helium buffer gas at 2−5 Torr (depending on the temperature). A short (50−100 μs) pulse of electrosprayed ions is injected into the drift tube; they travel through the drift tube under the influence of a weak electric field and exit through a small aperture. The ions that exit the drift tube are focused into a quadrupole mass spectrometer, and the arrival time distribution of the mass-selected ions is recorded at the detector. The arrival time distribution is then corrected to give the drift time distribution (the time that the ions spend traveling across the drift tube) by accounting for the flight time outside the drift tube. Measurements were performed with injection energies (the energy used to inject the ions into the drift tube) of 200−600 eV and drift voltages (the voltage across the drift tube) of 280−480 eV. $A_4G_7A_4$ and Ac-$A_4G_7A_4$ were synthesized using FastMoc (a variant of Fmoc) chemistry on an Applied Biosystems model 433A peptide synthesizer. The peptides were electrosprayed from solutions prepared by dissolving ∼2 mg of peptide in 1 mL of trifluoracetic acid and 0.1 mL of water.

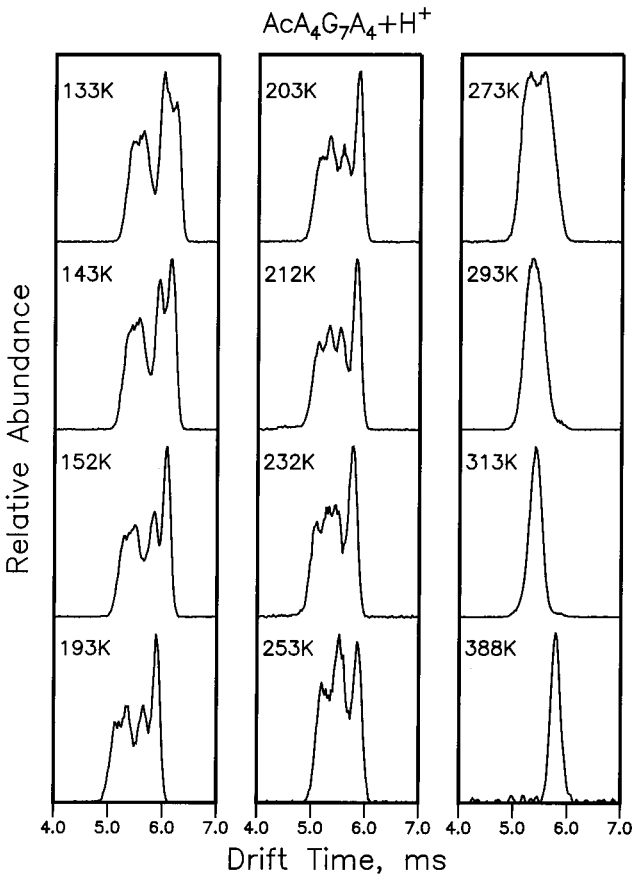

Figure 1. Drift time distributions measured for Ac-$A_4G_7A_4 + H^+$ over the temperature range examined (100−410 K). The measurements were performed with an injection energy of 400 eV and a drift voltage of 380 V.

Experimental Results

Figure 1 shows drift time distributions recorded for Ac-$A_4G_7A_4 + H^+$ with a range of drift tube temperatures. These measurements were performed with an injection energy of 400 eV and a drift voltage of 380 V. Up to four peaks can be discerned in the lower temperature distributions. Below 133 K, the distributions remain essentially unchanged. There are two poorly resolved peaks with long drift times and a broad feature at short drift times. As the temperature is raised from 133 to 152 K, the abundance of the peak with the longest drift time increases, and then the relative intensities of the different components stay about the same until the temperature approaches 253 K. At ∼193 K, the broad feature at short drift times starts to separate into two poorly resolved peaks, and at 212 K, there are clearly four peaks in the drift time distribution. Between 193 and 253 K, the two inner features appear to move toward the center and coalesce, so that at 253 K there are three peaks present. Between 253 and 273 K, the peak with the longest drift time disappears, and at 273 K, only two poorly resolved peaks remain. As the temperature is raised to 293 K, the peak with the longer drift time again disappears leaving behind a single broad peak, which becomes narrower as the temperature is raised further. At ∼343 K, this peak has narrowed to the

(18) Ihara, S.; Ooi, T.; Takahashi, S. *Biopolymers* **1982**, *21* 131−145.
(19) Shoemaker, K. R.; Kim, P. S.; York, E. J.; Stewart, J. M.; Baldwin, R. L. *Nature* **1987**, *326*, 563−567.
(20) Blagdon, D. E.; Goodman, M. *Biopolymers* **1975**, *14*, 241−245.
(21) Daggett, V. D.; Kollman, P. A.; Kuntz, I. D. *Chem. Scr.* **1989**, *29A*, 205−215.
(22) Privalov, P. L. *Crit. Rev. Biochem. Mol. Biol.* **1990**, *25*, 281−305.
(23) Ma, B.; Tsai, C.-J.; Nussinov, R. *Biophys. J.* **2000**, *79*, 2739−2753.
(24) Hagen, D. F. *Anal. Chem.* **1979**, *51*, 870−874.
(25) Von Helden, G.; Hsu, M.-T.; Kemper, P. R.; Bowers, M. T. *J. Chem. Phys.* **1991**, *95*, 3835−3837.
(26) Clemmer, D. E.; Jarrold, M. F. *J. Mass Spectrom.* **1997**, *32*, 577−592.
(27) Hudgins, R. R.; Mao, Y.; Ratner, M. A.; Jarrold, M. F. *Biophys. J.* **1999**, *76*, 1591−1597.
(28) Kinnear, B. S.; Hartings, M. R.; Jarrold, M. F. *J. Am. Chem. Soc.* **2001**, *123*, 5660−5667.

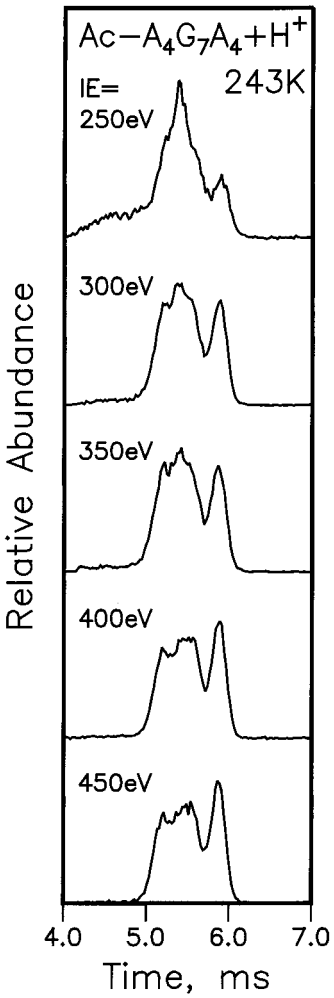

Figure 2. Drift time distributions measured for Ac-$A_4G_7A_4 + H^+$ at 243 K as a function of injection energy. The results shown here were recorded with a drift voltage of 380 V and with the temperature of the block surrounding the capillary interface lowered to 80 °C from its normal operating temperature of 100 °C.

point that it is close to the peak shape calculated for a single component.[29] This indicates that there is either only a single structure present or rapid conformational averaging occurs so that all ions sample the same time-averaged structure during their drift time. The latter interpretation is the more likely.

In the experiments, the ions are injected into the drift tube from the outside and as they enter the drift tube they undergo a series of collisions with the buffer gas, which thermalizes their injection energy. During this process, the ions are collisionally heated and then once their injection energy is thermalized, they are rapidly cooled by further collisions with the buffer gas.[30,31] Raising the injection energy increases the collisional heating, and the injected ions can be heated to the point where they are hot enough to undergo conformational changes before they rapidly cool to the drift tube temperature. As illustrated in Figure 2, the drift time distributions depend on the injection energy. Conformational changes may also be induced in the heated capillary interface of the electrospray source.[32,33] Indeed, the

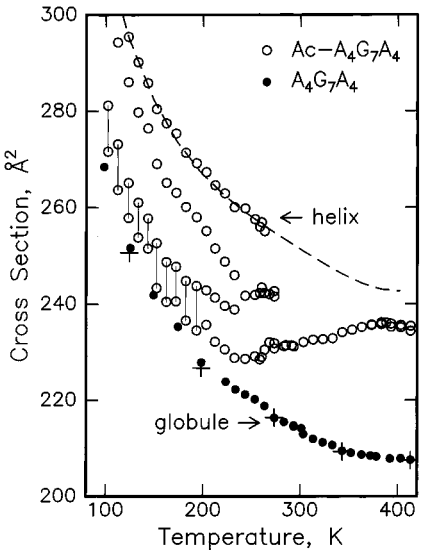

Figure 3. Plot of the cross sections for the main features in the drift time distributions for $A_4G_7A_4 + H^+$ (filled points) and Ac-$A_4G_7A_4 + H^+$ (open points) as a function of drift tube temperature. The results shown here were recorded with an injection energy of 400 eV and a drift voltage of 380 V. The thin vertical lines connect features that are not really resolved in the drift time distributions. The dashed line shows the expected behavior for the Ac-$A_4G_7A_4 + H^+$ α-helix. This was derived by fitting and scaling the cross sections for the features assigned to α-helical conformations for Ac-$A_5G_5A_5 + H^+$ and Ac-$A_6G_3A_6 + H^+$. For these peptides (which have more alanines and fewer glycines), the α-helix persists over virtually the entire temperature range studied. The large pluses show cross sections recorded for the Ac-$KG_{15} + H^+$ peptide which is expected to be globular throughout the entire temperature range studied.

results shown in Figure 2 were recorded with the temperature of the block surrounding the capillary interface lowered to 80 °C. With this temperature set at 100 °C, the substantial changes evident in the drift time distributions as the injection energy was lowered (see Figure 2) were not observed, presumably because the conformational changes were already induced in the heated capillary. At the lowest injection energy in Figure 2 (250 eV), there is a low-intensity shoulder at drift times between 4 and 5 ms; this is due to a doubly charged dimer (which has the same mass-to-charge ratio as the singly charged monomer). As the injection energy is raised above 250 eV, the relative abundance of the peak with the longest drift time increases. These results suggest that this feature is not present in solution but is formed in the gas phase. As will become evident, this feature is assigned to an α-helix. The α-helix is not expected to be abundant for the Ac-$A_4G_7A_4 + H^+$ peptide in solution because of the large block of glycines in the middle.

The measured drift times are easily converted into collision cross sections.[29] Figure 3 shows a plot of the cross sections determined for the main features observed in the drift time distributions for $A_4G_7A_4 + H^+$ and Ac-$A_4G_7A_4 + H^+$ peptides as a function of drift tube temperature. The results shown here were recorded with an injection energy of 400 eV and a drift voltage of 380 V. Only a single peak is observed for $A_4G_7A_4 + H^+$ over the entire temperature range studied (100−410 K). At room temperature and above, this peak has a width close to that calculated for a single component,[29] indicating that there is either only a single structure present or rapid conformational averaging occurs so that all ions sample the same time-averaged

(29) Mason, E. A.; McDaniel, E. W. *Transport Properties of Ions in Gases*; Wiley: New York, 1988.
(30) Jarrold, M. F.; Honea, E. C. *J. Phys. Chem.* **1991**, *95*, 9181−9185.
(31) Jarrold, M. F.; Honea, E. C. *J. Am. Chem. Soc.* **1992**, *114*, 459−464.
(32) Rockwood, A. L.; Busman, M.; Udseth, H. R.; Smith, R. D. *Rapid Commun. Mass Spectrom.* **1991**, *5*, 582−585.
(33) Li, J. W.; Taraszka, J. A.; Counterman, A. E.; Clemmer, D. E. *Int. J. Mass Spectrom.* **1999**, *187*, 37−47.

structure as they travel through the drift tube. As the temperature is lowered below room temperature, the peak gradually broadens beyond that expected for a single component. This indicates that the ions are becoming trapped in slightly different conformations during their time in the drift tube. As will become clear below, the feature observed for $A_4G_7A_4 + H^+$ is due to a globular conformation. The systematic decrease in the cross sections for this feature with increasing temperature (see Figure 3) results because (i) the long-range attractive interactions between the peptide ion and the buffer gas become less important with increasing temperature and (ii) the collisions ride further up the repulsive repulsive part of the intermolecular potential at higher temperature, leading to a shorter distance of closest approach. This systematic decrease in the cross sections is always expected to occur, though it may be combined with changes in the cross section that result from conformational changes with temperature.

For the $Ac\text{-}A_4G_7A_4 + H^+$ peptide, four features are shown in Figure 3 at temperatures less than ~230 K. Below ~200 K, the two peaks with the shortest drift times are not really resolved in the drift time distributions (see Figure 1), and in recognition of this, the points for these features are joined by a line. We show two sets of points here because there is clearly more than one feature present at short drift times in the low-temperature distributions (see Figure 1). Below ~250 K, the smallest cross sections for $Ac\text{-}A_4G_7A_4 + H^+$ are close to those for the $A_4G_7A_4 + H^+$ peptide, and so they are assigned to a globule. The cross sections for the $Ac\text{-}A_4G_7A_4 + H^+$ globule are slightly larger than for the $A_4G_7A_4 + H^+$ globule because of the acetyl group in the former. The largest $Ac\text{-}A_4G_7A_4 + H^+$ cross sections are (based on our previous work) close to the values expected for an α-helix (this assignment will be confirmed below). As the temperature is raised above 230 K, a series of changes occur. Above ~230 K, the middle two features for $Ac\text{-}A_4G_7A_4 + H^+$ coalesce. At ~265 K, the feature with the largest cross section (assigned to the α-helix) disappears. Then at ~275 K, the middle feature also disappears, apparently leaving behind the one originally assigned to the $Ac\text{-}A_4G_7A_4 + H^+$ globule. As the temperature is raised further, the cross sections for the remaining feature shift further and further away from those of the $A_4G_7A_4 + H^+$ globule. At ~400 K, the cross sections for this feature are quite close to the values expected for the α-helical conformation of $Ac\text{-}A_4G_7A_4 + H^+$, which is represented by the dashed line in the figure. The dashed line was derived by fitting and scaling the cross sections for the features assigned to α-helical conformations for $Ac\text{-}A_5G_5A_5 + H^+$ and $Ac\text{-}A_6G_3A_6 + H^+$. For these peptides (which have more alanines and fewer glycines), the α-helix persists over virtually the entire temperature range studied.

Molecular Dynamics Simulations: Methods

A series of molecular dynamics simulations were performed for the $A_4G_7A_4 + H^+$ and $Ac\text{-}A_4G_7A_4 + H^+$ peptides in order to obtain conformations for comparison with the experimental results presented above. The simulations were performed using the MACSIMUS suite of programs,[34] with the CHARMM force field (21.3 parameter set)[35] and a dielectric constant of 1.0. The temperature was maintained by rescaling the kinetic energies every 0.1 ps. Several different types of simulations were performed for both peptides: 960-ps simulations at 300 K starting from an ideal α-helix and simulated annealing with a schedule of 240 ps at 600, 500, and 400 K and 480 ps at 300 K starting from an ideal α-helix and an extended string. The latter usually yielded globular conformations. The linear-stepped annealing schedule employed here seemed to provide consistently lower energy structures in our previous work on similar peptides.[16] For the $Ac\text{-}A_4G_7A_4 + H^+$ peptide, simulated annealing and 960-ps 300 K simulations were also performed starting from the "special" helical structure recently found in simulations for $Ac\text{-}(AGG)_5K + H^+$ (a partially untwisted helix with predominantly $i, i + 6$ hydrogen bonding and a row of hydrogen bonds that point backward with respect to those in a conventional right-handed helix).[28] We usually run many (often up to 50) simulations starting from the same conformation. Ideally, one would like to run the simulations for as long as possible, but the simulation times employed here are a compromise that takes into account their computational expense. Average potential energies and average collision cross sections were obtained from the final 35 ps of each simulation. Cross sections were calculated using an empirical correction to the exact hard-spheres scattering model,[17] averaging over 50 snapshots taken from the final 35 ps of each simulation. If the conformation is correct in the simulation, the calculated cross sections are expected to be within 2% of the measured values.

In addition to the simulations described above, a number of simulations were performed for the $Ac\text{-}A_4G_7A_4 + H^+$ peptide with different terminal temperatures. A series of 10 960-ps simulations, starting from an ideal α-helix, were performed at 150, 200, 250, 300, 350, and 400 K. We also did a series of simulations where the final conformation from one simulation was used as the initial conformation for the next lower temperature one. Thus, 10 960-ps simulations were performed at 400 K, starting from an ideal α-helix, and then the final conformations were used as the initial conformations for 10 350 K, 960-s simulations, and so on down to 150 K. As in the other simulations, the average potential energies and average collision cross sections were obtained from the final 35 ps. But here the cross sections were calculated using the trajectory method,[36] averaging over 50 snapshots from the final 35 ps of each simulation. In the trajectory method, the cross section (or more correctly the collision integral) is calculated by averaging a function of the scattering angle (the angle between the incoming and outgoing trajectory in a collision between the ion and buffer gas atom) over relative velocity and collision geometry. The scattering angles are determined from trajectory calculations using a summed Lennard-Jones plus charge-induced dipole potential between the ion and buffer gas atom.[37] The trajectory calculations consume large amounts of computer time, but this

(34) Kolafa, J. http://www.icpf.cas.cz/jiri/macsimus/default.htm
(35) Brooks, B. R.; Bruccoleri, R. E.; Olafson, B. D.; States, D. J.; Swaminathan, S.; Karplus, M. *J. Comput. Chem.* **1983**, *4*, 187−217.
(36) Mesleh, M. F.; Hunter, J. M.; Shvartsburg, A. A.; Schatz, G. C.; Jarrold, M. F. *J. Phys. Chem.* **1996**, *100*, 16082−16086.
(37) The Lennard-Jones parameters employed were $\epsilon_o = 0.65$ meV and $\sigma = 2.38$ Å for H−He interactions and $\epsilon_o = 1.34$ meV and $\sigma = 3.042$ Å for C−He and all other atoms. Here ϵ_o is the depth of the potential and σ is the distance where it passes through zero. The C−He parameters were obtained by fitting the mobility for C_{60}^+ over a broad temperature range. The same parameters account for the mobilities of carbon chains and rings. For H−He, the ϵ_o is an average from ab initio calculations and the σ is from fitting mobilities of $C_6H_6^+$ and other hydrocarbon ions. The H−He interactions are by far the most important, because hydrogen covers most of the surface of the peptides. For the charge induced-dipole part of the potential, the partial charges from the CHARMM force field were employed.

approach is necessary to correctly account for the temperature dependences of the cross sections.

We have not yet addressed the issue of the protonation sites in the $A_4G_7A_4 + H^+$ and Ac-$A_4G_7A_4 + H^+$ peptides. For reasons that will be discussed below, we assume that $A_4G_7A_4 + H^+$ is protonated at the N-terminus. For Ac-$A_4G_7A_4 + H^+$, the N-terminus is blocked by acetylation and so the amide CO groups are probably the preferred protonation sites. In principle, any one of the amide CO groups may be protonated; however, protonation near the C-terminus will be preferred for the helices. We performed simulations with the protonation site at the amide CO nearest the C-terminus, nearest the N-terminus, and in the middle. After the amide CO groups, the carboxyl CO group is expected to have the next largest proton affinity.[38] We performed some simulations with the carboxyl CO protonated because this protonation site may be preferred for Ac-$A_4G_7A_4 + H^+$ helices. The charge is closer to the C-terminus than when the amide CO nearest the C-terminus is protonated, which may allow for more favorable interactions with the helix dipole. The results, however, were not substantially different from those for Ac-$A_4G_7A_4 + H^+$ protonated at the amide CO. The same three main conformations were found (α-helix, partial π-helix, globule), and in particular, there was no significant enhancement in the stability of the helices over the globule when the carboxyl CO is protonated. This indicates that protonation at the carboxyl CO does not stabilize the helix significantly more than protonation at the amide CO nearest the C-terminus. The proton affinity of the carboxyl CO is expected to be substantially smaller than for the amide CO[38] and so protonation at the carboxyl CO seems unlikely even for helices. We will briefly mention these results further below.

The simulations reported here were performed with a classical force field. Even single-point energy calculations using either density functional theory or quantum chemistry methods are not really feasible for peptides of the size considered here because in order to get a reasonably accurate representation of the weak interactions responsible for defining their conformations, very large basis sets are required. Since it is also necessary to consider the dynamic aspects of these floppy molecules, there is really no alternative to using a classical force field along with MD simulations. There is a concern that a classical force field is not accurate enough. While the force field employed here, CHARMM, was calibrated specifically for peptides and proteins, it is a relatively simple one, incorporating only electrostatic, Lennard-Jones, and internal bonding terms (hydrogen bonds, which are primarily electrostatic in nature, are included in the electrostatic term). The force field used here is not polarizable[39] and does not account for environment effects.[40] There is also a concern that it may overemphasize some interactions, while other weak interactions, such as the C^{α}—H···O═C hydrogen bond,[41] are missing. For these reasons, the accuracy of the energies and conformations obtained from the force field should be considered. Like all other methods, a classical force field will probably fare worse when the energies of two conformations that are quite different are compared (for example, a helix and globule). Indeed, the work presented here provides an example of where the force field calculations appear to get the ordering of such different conformations wrong (see below). We should, however, note that the Ac-$A_4G_7A_4 + H^+$ peptide was designed to have a flat energy landscape, and a reversal in the ordering of two confomations that have almost the same energy is not unexpected. As with other methods, the energy differences associated with small variations around a particular conformation are probably more reliable than those involving large conformational differences. It is still possible to get the geometries almost right even if they have the wrong energy ordering.[42] Indeed, this is often observed with other methods. In this regard, the force field may fare better than many more sophisticated theoretical approaches. It is difficult to get all the weak interactions that define a conformation right from first principles, but the force field is parametrized to give the right average bond lengths and angles. In other words, the force field may get the relative energy of an α-helix wrong, but it will probably get the structure right in an average sense because of the way it is parametrized. Where the force field may fail to get the structure right is if an unusual bonding scheme plays an important role in defining the conformation. Such behavior is obviously difficult to predict without the benefit of high-level calculations.

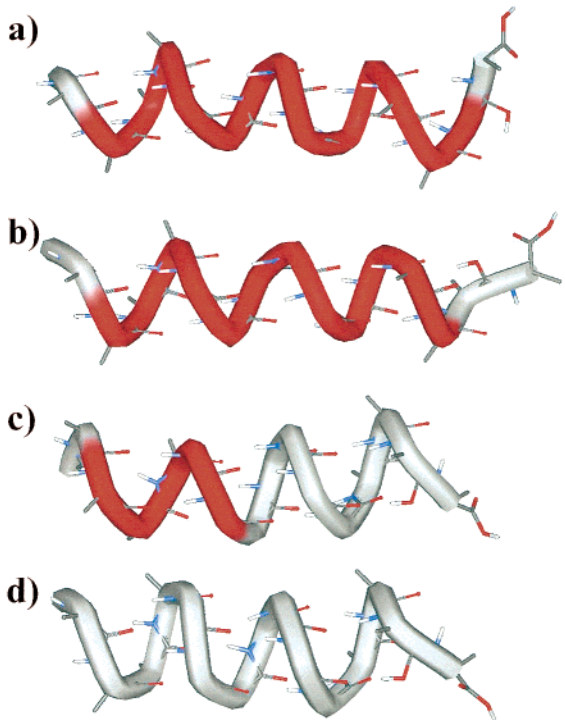

Figure 4. Examples of helical conformations found in the molecular dynamics simulations for Ac-$A_4G_7A_4$ protonated at the amide CO nearest the C-terminus. All conformations are from 300 K simulations or simulations that terminated at 300 K. (a) shows an α-helix with the C-terminus tucked in, (b) shows an α-helix with the C-terminus extended, (c) shows a partial α/partial π-helix, and (d) shows a π-helix. The images were produced using the WebLab viewer (Molecular Simulations Inc., San Diego, CA). α-Helical regions are red, and β-sheet regions are blue.

Molecular Dynamics Simulations: Results

Figure 4 shows examples of some of the helical conformations found in the MD simulations for Ac-$A_4G_7A_4 + H^+$ protonated

(38) Zhang, K.; Cassady, C. J.; Chung-Phillips, A. *J. Am. Chem. Soc.* **1994**, *116*, 11512−11521.
(39) Banks, J. L.; Kaminski, G. A.; Zhou, R. H.; Mainz, D. T.; Berne, B. J.; Friesner, R. A. *J. Chem. Phys.* **1999**, *110*, 741−754.
(40) Rick, S. W.; Cachau, R. E. *J. Chem. Phys.* **2000**, *112*, 5230−5241.
(41) Vargas, R.; Garza, J.; Dixon, D. A.; Hay, B. P. *J. Am. Chem. Soc.* **2000**, *122*, 4750−4755.
(42) Jensen, F. *Introduction to Computational Chemistry*; John Wiley and Sons Ltd.: Chichester, England, 1999.

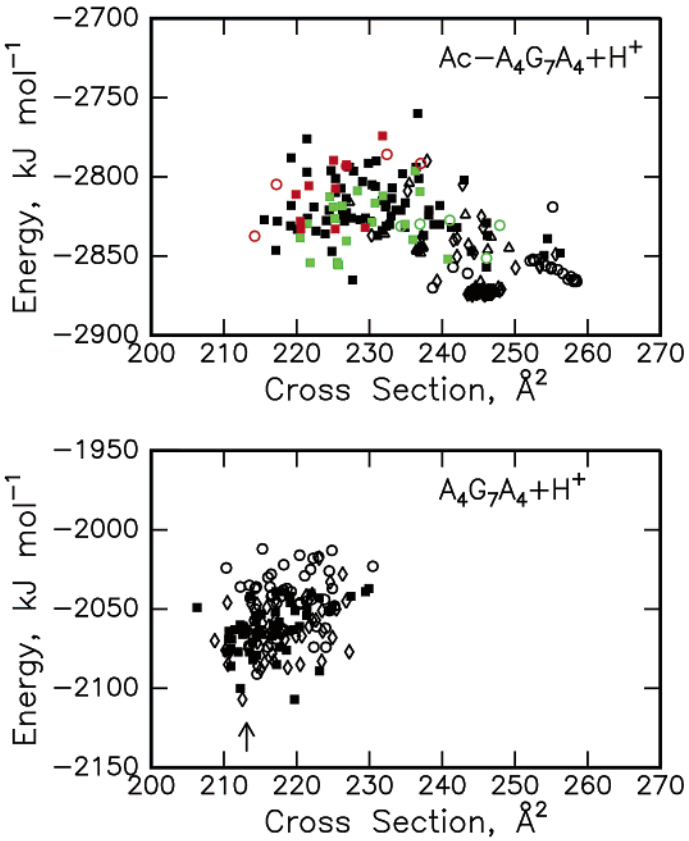

Figure 5. Plot of energy against cross section for Ac-$A_4G_7A_4 + H^+$ and $A_4G_7A_4 + H^+$ simulations. All results are from 300 K simulations or simulations that terminated at 300 K. The upper plot shows results for Ac-$A_4G_7A_4 + H^+$ protonated at the amide CO nearest the N-terminus (red), the middle amide CO (green), and the amide CO nearest the C-terminus (black). The lower plot shows results for $A_4G_7A_4 + H^+$ protonated at the N-terminus. Key: filled square, simulated annealing from linear start; open diamond, simulated annealing from α-helical start; open circle, 960-ps 300 K MD from α-helical start; open triangle, 960-ps 300 K MD and simulated annealing from special helix (see text) start.

at the amide CO nearest the C-terminus. Conformations a and b in Figure 4 are α-helices; (a) is close to an ideal α-helix while in (b) the C-terminus is twisted out and the protonated amide CO group is twisted around so that it can hydrogen bond to other carbonyl groups. In the simulations, (b) is ∼11 kJ mol^{-1} lower in energy than (a), and their calculated cross sections are significantly different (see below). Conformations c and d in Figure 4 are partial π-helices. They have conformations that lie between an ideal α-helix and ideal π-helix. A α-helix has i, $i + 5$ hydrogen bonds (4.4 residues/turn) while an α-helix has i, $i + 4$ hydrogen bonds (3.6 residues/turn). Figure 4c is an α-helix at the N-terminus end and a π-helix at the C-terminus end. The π-helix may be favored at the C-terminus because it provides an extra carbonyl group to hydrogen bond to the protonated CO, while the α-helix persists at the N-terminus presumably because it has one fewer dangling N−H group than the π-helix. Figure 4d is closer to an ideal π-helix, but (c) and (d) have similar cross sections and energies. The partial π-helices have energies that are ∼10 kJ mol^{-1} lower than the lowest energy α-helix found in the simulations.

Figure 5 shows plots of the energy against cross section for all the 300 K simulations and the simulations terminating at 300 K (except for Ac-$A_4G_7A_4 + H^+$ protonated at the carboxyl CO). The upper plot shows results for Ac-$A_4G_7A_4 + H^+$ protonated at one of the amide COs. The black points show the results obtained with the amide CO nearest the C-terminus protonated. The group of points with energies at ∼−2875 kJ mol^{-1} and cross sections at ∼243−248 $Å^2$ are partial π-helices. The couple of points with cross sections at ∼239 $Å^2$ and energies at ∼−2870 kJ mol^{-1} are also partial π-helices, but they have the C-terminus carboxyl group folded in, and so they are slightly more compact. The group of points with energies around −2850 to −2870 kJ mol^{-1} and cross sections between 252 and 258 $Å^2$ are α-helices. The points with the smaller cross sections and higher energies have conformations like Figure 4a, while the points with lower energies and larger cross sections have conformations like Figure 4b. In contrast to the results described here, only a single type of α-helix was found in the simulations for Ac-$A_4G_7A_4 + H^+$ protonated at the carboxyl CO. These helices have cross sections at ∼252 $Å^2$, which is at the low end of the range mentioned above. Clearly, the conformation at the C-terminus is affected by where the ion is protonated. Partial π-helices are also observed when the carboxyl CO is protonated; however, here the α- and partial π-helices are almost isoenergetic.

Figure 6 shows examples of some of the other conformations found in the simulations for Ac-$A_4G_7A_4 + H^+$ protonated at the amide CO nearest the C-terminus. Figure 6a shows a typical conformation from simulations started from a geometry close to the "special" helical structure of Ac−$(AGG)_5K + H^+$ (a partially untwisted helix with predominantly i, $i + 6$ hydrogen bonding and a row of three backward-pointing hydrogen bonds).[28] While this is the lowest energy conformation found in the Ac-$(AGG)_5K + H^+$ simulations, it is not particularly low in energy for Ac-$A_4G_7A_4 + H^+$. The open triangles clustered around −2845 kJ mol^{-1} and 237 $Å^2$ in Figure 5 are from 300

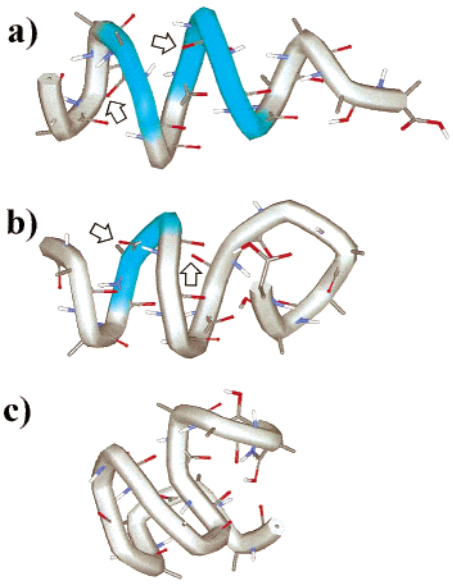

Figure 6. Examples of partially helical and globular conformations found in the molecular dynamics simulations for Ac-$A_4G_7A_4$ protonated at the amide CO nearest the C-terminus. All conformations are from 300 K simulations or simulations that terminated at 300 K. (a) shows an example of what results from starting the simulations from a conformation close to the "special" Ac-$(AGG)_5K + H^+$ helix (see text), (b) shows the lowest energy globular conformation found in the simulations, and (c) shows one of the most compact globular conformations found in the simulations. Small arrows indicate the "backward" pointing carbonyl groups in (a) and (b). The images were produced using the WebLab viewer (Molecular Simulations Inc., San Diego, CA). α-Helical regions are red, and β-sheets regions are blue.

K simulations started from a geometry close to the "special" Ac-$(AGG)_5K + H^+$ structure. The conformation at the end of these simulations is significantly removed from the starting conformation, providing more evidence that the "special" Ac-$(AGG)_5K + H^+$ structure is not a favored structure for Ac-$A_4G_7A_4 + H^+$. The geometry at the C-terminus is quite different from that found for Ac-$(AGG)_5K + H^+$, though there are still two backward-pointing hydrogen bonds, which are indicated by arrows in Figure 6a.

Figure 6b shows the lowest energy globule found in the MD simulations for Ac-$A_4G_7A_4 + H^+$ protonated at the amide CO nearest the C-terminus. This conformation has an energy of -2865 kJ mol^{-1} and a cross section of 228 Å^2. Its geometry has some features in common with that shown in Figure 6a: it is partially helical and has two backward-pointing hydrogen bonds. Figure 6c shows an example of a more compact globular conformation. This conformation has an energy of -2828 kJ mol^{-1} and a cross section of 217 Å^2. The cross section of the more compact conformation is in better agreement with the measured value for the Ac-$A_4G_7A_4 + H^+$ globule extrapolated to 300 K ($\sim$219 Å^2).

The green points in Figure 5 show results for Ac-$A_4G_7A_4 + H^+$ protonated at the amide CO in the middle, while the red points show results for Ac-$A_4G_7A_4 + H^+$ protonated at the amide CO nearest the N-terminus. Moving the charge away from the C-terminus and toward the N-terminus destabilizes the helices. With the charge at the N-terminus, only globular conformations are found. While there is a definite preference for protonation at the C-terminus for the helical conformations, there is no obvious preference for a particular protonation site for the globular conformation. The proton may even be mobile in the globules (jumping between different carbonyl groups), which is a possibility that is not incorporated in the MD simulations. A "mobile proton" model has been proposed to account for the apparent mobility of the protons in the dissociation of some collisionally excited peptide ions.[43] The fragmentation of protonated peptides is believed to be charge-induced. A strongly localized charge leads to only a few fragment ions, while a large number of fragments indicates either a heterogeneous mixture where the peptide is protonated at different sites[44] or a mobile proton hopping between the different protonation sites. It is usually assumed that there is an energetic penalty associated with mobilizing the proton from a basic site and that the proton is only mobile when the ion is collisionally heated. In the Ac-$A_4G_7A_4 + H^+$ peptide, where any one of the backbone CO groups could be protonated, it is in principle possible that the proton is mobile under the conditions in the drift tube (where the maximum temperature is not substantially above room temperature). On the other hand, the simulations show that the protonated CO becomes surrounded by, and hydrogen bonded to, other backbone CO groups. If the proton hops to another site, this "self-solvation shell" must be reorganized. The activation energy associated with this reorganization may severely restrict or even prohibit proton mobility.

The lower half of Figure 5 shows results obtained for $A_4G_7A_4 + H^+$ protonated at the N-terminus. All these simulations collapsed to a globule, including the 300 K simulations started from an ideal α-helix. The arrow in the figure shows the measured cross section for the $A_4G_7A_4 + H^+$ peptide at 300 K. The cross sections calculated for the globular conformations from the MD simulations are close to the measured value, indicating that $A_4G_7A_4 + H^+$ is globular at 300 K. The measured cross section for the $A_4G_7A_4 + H^+$ peptide is on the low end of the range of calculated cross sections. This may result because of the difficulty in finding compact low-energy globules in the simulations (see below).[16] There is, however, no ambiguity about the assignment of a globular conformation to $A_4G_7A_4 + H^+$ because the globule is the most compact state.

Figure 7 shows cross sections calculated for Ac-$A_4G_7A_4 + H^+$ helices as a function of temperature. The final conformations are separated into α-helices and partial π-helices. The circles represent simulations performed at a single fixed temperature, while the triangles are for simulations started at 400 K and stepped-down in 50 K increments. For the latter, the partial π-helix is the dominant conformation at all final temperatures. For the simulations performed at a single fixed temperature, the partial π-helix is the dominant conformation at the upper end of the temperature range, while the α-helix (the starting conformation) persists at low temperatures. As mentioned above, there are two types of α-helix for Ac-$A_4G_7A_4 + H^+$ protonated at the amide CO nearest the C-terminus corresponding to (a) and (b) in Figure 4. At low temperatures, most simulations remain trapped in the slightly higher energy (a) form, which is closer to the ideal α-helical starting point. At higher temperatures, the (b) form, which has the larger cross section, becomes dominant. The transition from the (a) form to the slightly lower energy (b) form occurs within the 960-ps time frame of the simulations at 200−250 K, while the α-helix converts into the

(43) Dongre, A. R.; Jones, J. L.; Somogyi, Á.; Wysocki, V. H. *J. Am. Chem. Soc.* **1996**, *118*, 8365−8374
(44) Burlet, O.; Orkiszewski, R. S.; Ballard, K. D.; Gaskell, S. J. *Rapid Commun. Mass Spectrom.* **1992**, *6*, 658−662.

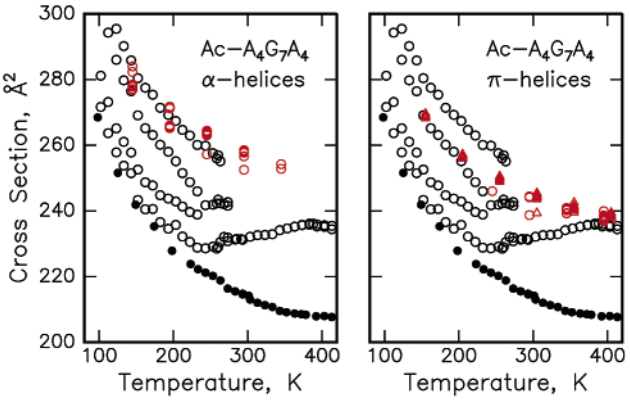

Figure 7. Comparison of measured cross sections (black points) with cross sections calculated for helical conformations of Ac-$A_4G_7A_4 + H^+$ protonated at the amide CO nearest the C-terminus (red points). The red circles show the results for 960-ps simulations performed at 150, 200, 250, 300, 350, and 400 K starting from an ideal α-helix. The red triangles show the results for 960-ps simulations where the final conformation from one simulation was used as the initial conformation for the next lower temperature (starting at 400 K with an ideal α-helix). The first set of simulations (red circles) may become trapped in higher energy helical conformations while the second set (red triangles) should anneal into the lowest free energy helix at each temperature. The dashed line shows the expected behavior for the Ac-$A_4G_7A_4 + H^+$ α-helix, which was derived by fitting and scaling the cross sections for the Ac-$A_5G_5A_5 + H^+$ and Ac-$A_6G_3A_6 + H^+$ α-helices. The thin vertical lines connect features that are not really resolved in the drift time distributions.

slightly lower energy partial π-helix at 300−350 K. There is no evidence in the experimental results for the two types of α-helix found in the MD simulations. It is possible that the rate of interconversion between the two forms is fast on the experimental time scale, even at low temperatures.

The calculated cross sections do a reasonably good job of reproducing the measured temperature dependences (see Figure 7). The small discrepancies that are present (the temperature dependences for the α-helix seem to be slightly underestimated) may result from inadequacies in the summed Lennard-Jones plus ion-induced dipole potential used to model the intermolecular interactions between the ion and the buffer gas.[37] On the other hand, the discrepancies may indicate that a more complex behavior (such as a conformational change) is occurring. For example, the cross sections for the larger type of α-helix shown in Figure 4b appear to fit the measured cross sections better at low temperature, while the cross sections for the smaller type of α-helix shown in Figure 4a are a better fit at the middle of the temperature range studied. So a gradual transition from the larger type of helix to the smaller with increasing temperature would provide an excellent fit to the experimental data. There is, however, no other evidence to indicate that this is occurring.

Discussion

The $A_4G_7A_4 + H^+$ peptide shows a single peak throughout the temperature range examined, and as described above, comparison with cross sections from MD simulations shows that $A_4G_7A_4 + H^+$ is a globule at 300 K. The large pluses in Figure 3 show cross sections measured for the Ac-$KG_{15} + H^+$ peptide as a function of temperature. Glycine has low propensities to form either α-helices[12] or β-sheets[45] and so the Ac-$KG_{15} + H^+$ peptide is expected to adopt a globular conformation throughout the whole temperature range examined. Cross sections for the $A_4G_7A_4 + H^+$ peptide closely track those for Ac-$KG_{15} + H^+$. This provides a strong indication that the $A_4G_7A_4 + H^+$ peptide also retains the same conformation throughout the whole temperature range. Since the $A_4G_7A_4 + H^+$ peptide has already been shown to be globular at 300 K, it must be globular at all temperatures studied.

In solution, the most basic site in the $A_4G_7A_4$ peptide is the N-terminus. In the gas phase, the proton affinities of the amide CO groups and the N-terminus are expected to be close, and it is possible that the N-terminus is not the most basic site. In recent density functional theory calculations for $G_3 + H^+$, several low-energy structures were found with the proton located at the N-terminus and at the amide CO group nearest the N-terminus.[46] The lowest free-energy structure found in this study is protonated at the N-terminus amide CO and has an O−H···N hydrogen bond to the nitrogen atom at the N-terminus. Conformations with the N-terminus protonated are essentially isoenergetic in the calculations. However, protonation at the other amide CO group was found to be significantly less favorable. So, according to the most recent calculations, the preferred protonation sites for G_3 are either at or near the N-terminus.

The failure to observe any helical conformations for the $A_4G_7A_4 + H^+$ peptide is consistent with protonation at or near the N-terminus where unfavorable interactions between the charge and the helix macrodipole disrupt helix formation. The $A_4G_7A_4 + H^+$ ions remain in a globular conformation even when injected into the drift tube with injection energies of up to 600 eV (which is well above the injection energy required to induce conformational changes in the Ac-$A_4G_7A_4 + H^+$ peptide). In the experiments, the ions are collisionally heated and then rapidly cooled as they enter the drift tube. This transient heating and cooling cycle is fast and occurs close to the entrance of the drift tube.[30,31] At high injection energies, the $A_4G_7A_4 + H^+$ ions may become hot enough that the proton becomes mobile. However, if this happens, the proton must return to be near the N-terminus when the ions cool, because there is no sign of the helical conformations that should result from protonation near the C-terminus. Similar behavior has been observed for a wide range of unacetylated peptides, including, for example, protonated polyalanine[27] which only becomes helical when the N-terminus is acetylated.[16] The most reasonable explanation for this behavior is that the proton is pinned to the N-terminus in the unacetylated peptide.

For Ac-$A_4G_7A_4 + H^+$, where protonation at the N-terminus is blocked, at least four different conformations are observed at low temperatures (<230 K). The one with the smallest cross section is globular, from comparison with $A_4G_7A_4 + H^+$, while the two conformations with the largest cross sections are attributed to α- and partial π-helices from comparisons with the results of the MD simulations. Both types of helices (α and partial π) have been found before in different peptides;[14,17] however, this is the first time that they have both been found in the same peptide. The structure of the other main Ac-$A_4G_7A_4 + H^+$ conformation (the one with a cross section slightly larger than the globule) is not known at present. The fact that there is no analogue of this feature for the $A_4G_7A_4 + H^+$ peptide is consistent with it having some helical character. It may have a

(45) Smith, C. K.; Regan, L. *Acc. Chem. Res.* **1997**, *30*, 153−161.

(46) Rodriquez, C. F.; Cunje, A.; Shoeib, T.; Chu, I. K.; Hopkinson, A. C.; Siu, K. W. M *J. Am. Chem. Soc.* **2001**, *123*, 3006−3012.

structure close to that shown in Figure 6b, this partially helical conformation is both low in energy and has close to the right cross section to match the measured values.

For the two features assigned to α- and partial π-helices there appear to be no other viable candidate structures, at least from the MD simulations. Most of the more extended conformations (cross sections >240 Å^2) found in the MD simulations for Ac-$A_4G_7A_4$ + H^+ are helical or partially helical. These higher energy helices often have one of their ends trapped in an unfavorable arrangement. A β-hairpin may have a cross section close to those assigned to the helices. A β-hairpin, a fragment of a β-sheet, consists of a turn and two short antiparallel β-strands. However, this conformation has not appeared to be viable in the gas phase for peptides in the size range studied here, even when the peptide in question has a large proportion of amino acids with high propensities to form β-sheets.[17] Both β-hairpins and β-sheets need to be stabilized by side-chain interactions. Neither glycine nor alanine is a good sheet former,[45] and so the β-hairpin is not a viable structure for Ac-$A_4G_7A_4$ + H^+.

The observation of several distinct conformations at temperatures below 230 K is consistent with the view that at low temperatures the rate of interconversion between the different Ac-$A_4G_7A_4$ + H^+ conformations is slow compared to the experimental time scale: the different conformations are effectively "frozen-out". As the temperature is raised, the conformations start to interconvert. First, the middle two peaks coalesce. If the assignments given above are correct, this represents the onset of rapid interconversion between the π-helix and the partially helical structure. At a slightly higher temperature, the peak attributed to the α-helix disappears. It is not clear what the α-helix converts into, partly because at slightly higher temperature the feature resulting from the coalescence of the π-helix and the partially helical structure also disappears or coalesces leaving behind the peak originally assigned to the globule. However, this peak is slightly displaced from the position expected for an ideal globule, suggesting that the resulting conformation may incorporate some helical character. Ultimately, all the different conformations that are "frozen-out" at low temperatures convert into this conformation when the temperature is raised.

At this point it is useful to consider the origin of the α-helical conformation observed at low temperature. The Ac-$A_4G_7A_4$ peptide is not expected to be helical in solution (it contains too many glycine residues and it is in a strongly acidic solution), so it seems that the helix must form in the gas phase. Raising the capillary temperature and raising the injection energy both lead to more helix. The effect of raising the injection energy on the abundance of the helix is evident from Figure 2. These results suggest that the helix forms when the Ac-$A_4G_7A_4$ + H^+ ions are hot from being injected into the drift tube, and it is "frozen-out" when the peptide ions are rapidly cooled to the buffer gas temperature shortly after entering the drift tube.

Additional evidence that the helix is the preferred conformation at high temperature is evident in Figure 3. As the temperature is raised above 250 K, the peak assigned to the Ac-$A_4G_7A_4$ + H^+ globule moves further away from the position expected for a globule (close to the $A_4G_7A_4$ + H^+ cross sections) to the position expected for a helix. The narrowing of the peak that occurs in this temperature range (see above) suggests that interconversion between different conformations is starting to occur on a time scale that is fast compared to the time spent in the drift tube. Thus, the position of the peak reflects how long the peptide spends in each conformation. As the temperature is raised, the peak moves close to the position expected for the helix, indicating that the helix is the preferred conformation at the higher temperatures. It is not possible to say from our results whether this helix is predominantly an α-helix, is predominantly a π-helix, or represents a conformational equilibrium of both.

The idea that the helix is the favored conformation at high temperature while the globule has the lower free energy at low temperature is sufficiently radical that we should consider other possible interpretations of the results. It seems very unlikely that the large cross sections for the Ac-$A_4G_7A_4$ + H^+ peptide at 400 K could be due to some sort of distorted globule state. The globule is close to spherical because this maximizes its bonding interactions; to account for the measured cross sections, a distorted globule would need to have an aspect ratio like the helices in Figure 4. It also seems very unlikely that the increase in the cross section for the Ac-$A_4G_7A_4$ + H^+ peptide at the higher temperatures is due to a nonspecific unfolding process to a less compact random coillike structure. This behavior is not observed for the $A_4G_7A_4$ + H^+ peptide, for the Ac-KG_{15} + H^+ peptide, or in the simulations. Finally, we have now examined a number of related peptides designed to have marginally stable helical states. The increase in the helical content at high temperature is not just restricted to the Ac-$A_4G_7A_4$ + H^+ peptide but appears to be a fairly common phenomenon.

The transition from the globule being the preferred conformation at low temperatures to the helix at high temperatures is presumably driven by entropy: the helix must be favored entropically over the globule. Since the globule is expected to have a higher configurational entropy than the helix, the helix must have an enhanced vibrational entropy.[47] The globule is a compact and constrained geometry, and indeed, some recent calculations by Ma et al. suggest that the helix has a larger vibrational entropy than the globule because the helix has low-frequency longitudinal modes for which there are no counterparts in the globule.[23] While it is generally assumed that the globule should have a higher configurational entropy than the helix, the magnitude of the globule's configurational entropy is not known. The globule has a compact structure so its configurational entropy will be much less than for a random coil; there may well only be a few low-energy (enthalpy) globular states. So it is plausible that the enhanced vibrational entropy of the helix could overcome the larger configurational entropy of the globule. If this occurs (and the globule is slightly lower in energy than the helix), then the globule will be preferred at low temperature and the helix will be favored at high temperature. This seems to be the most plausible explanation for the experimental observations. Note that, if the preceding explanation is correct, there should be a helix-to-coil transition at significantly higher temperatures, where the random coil is an unfolded structure (unlike the globule) with a very large configurational entropy.

(47) By vibrational entropy we mean the vibrational entropy for a single well-defined structure (like the helix). The configurational entropy is the entropy resulting from the fact that a number of significantly different structures are accessible for some conformations (like the globule).

The complex conformational changes that occur with the Ac-$A_4G_7A_4 + H^+$ peptide as the temperature is changed seem to be poorly reproduced by the simulations. There is a transition from an α-helix to a π-helix as the temperature is raised, but the transitions to the globule that are present in the experiments are not evident in the simulations. The short time scale of the simulations may be at least partly responsible for the discrepancies. However, the globule is slightly higher in energy than the helices in the simulations (see Figure 5), and in order to explain our experimental observations (specifically that the globule is preferred at intermediate temperatures), the helices should be slightly higher in energy than the globule. It is possible that there are lower energy globules that have not been found in the simulations. As we have discussed elsewhere, it is difficult to find compact low-energy globule states by simulated annealing because significantly raising the temperature tends to drive the peptide to less compact conformations. In an effort to overcome these problems, we are currently implementing more sophisticated search methods based on evolutionary algorithms.

Conclusions

In this paper, we have reported studies of an unsolvated peptide designed to have a flat energy landscape with a marginally stable helical state. Several different conformations are "frozen-out" for the Ac-$A_4G_7A_4 + H^+$ peptide at low temperatures. These have been assigned to α- and partial π-helices, possibly a partially helical state, and a globule. As the temperature is raised, the different conformations begin to interconvert, and ultimately they all appear to convert into the globular conformation. As the temperature is raised further, the cross sections increase to become close to the values expected for helices. The only reasonable explanation for this increase in the cross sections with temperature is that it results from an increase in the helical content. The increase in the helical content with increasing temperature is attributed to the helix having a higher vibrational entropy than the globular conformation, as predicted by the calculations of Ma et al.[23]

Only a globular conformation was observed for the unacetylated $A_4G_7A_4 + H^+$ peptide throughout the whole temperature range examined. The persistence of the globular conformation for this peptide is accounted for by it being protonated at the N-terminus; this destabilizes the helix by unfavorable interactions between the charge and the helix macrodipole.

The results presented here show that even unsolvated peptides can display remarkably complex structural behavior. Indeed, the complex behavior found here could not easily be unraveled in conventional solution studies using, for example, cirular dichroism as the structural probe. The challenge now is to discover how the individual amino acid building blocks and their precise sequence influence the conformations observed for unsolvated peptides and to learn how to transfer this knowledge to other environments.

Acknowledgment. We thank Jiri Kolafa for use of his MACSIMUS molecular modeling programs and for his helpful advice. We gratefully acknowledge the support of the National Institutes of Health.

JA012150V